

Spectrum correction on Ekman-Navier-Stokes equation in two-dimensions

V.J. Valadão^{1*}, G. Boffetta¹, F. De Lillo¹, S. Musacchio¹, and M. Crialesi-Esposito²

¹*Dipartimento di Fisica and INFN - Università degli Studi di Torino,
Via Pietro Giuria, 1, 10125 Torino TO, Italy. and*

²*DIEF, University of Modena and Reggio Emilia, 41125 Modena, Italy.*

Abstract

The presence of a linear friction drag affects significantly the dynamics of turbulent flows in two-dimensions. At small scales, it induces a correction to the slope of the energy spectrum in the range of wavenumbers corresponding to the direct enstrophy cascade. Simple arguments predict that this correction is proportional to the ratio of the friction coefficient to the characteristic deformation rate of the flow. In this work, we examine this phenomenon by means of a set of GPU-accelerated numerical simulations at high resolutions, varying both the Reynolds number and the friction coefficient. Exploiting the relation between the energy spectrum and the enstrophy flux, we obtain accurate measurements of the spectral scaling exponents. Our results show that the exponent of the spectral correction follows a universal linear law in which the friction coefficient is rescaled by the enstrophy injection rate.

* Corresponding author: victor.dejesusvaladao@unito.it

I. INTRODUCTION

A significant number of natural fluid dynamical systems, such as atmospheric jet streams [1], ocean currents [2], and planetary flows [3], exhibit turbulent motion. While the turbulent flow is typically a three-dimensional (3D) phenomenon, many real-world phenomena display characteristics of two-dimensional (2D) turbulence across various scales. Examples of such 2D turbulence include large-scale patterns in the Earth's atmosphere [4], flows confined within thin fluid layers by geometric boundaries [5–8] and the behavior of conducting fluids under strong magnetic fields [9]. In contrast to 3D turbulence, where energy is transferred from larger to smaller scales in a forward cascade [10, 11], 2D turbulence is characterized by a dual cascade: an inverse energy cascade towards large scales and a direct cascade in which the enstrophy is transferred towards small scales [12, 13].

Linear friction, also referred to as Ekman friction, is commonly added to the Navier-Stokes (NS) equations in 2D as an essential ingredient for modeling real-world effects such as boundary layer dynamics, bottom drag in oceans, atmospheric resistance [1] or the air friction in experiments with soap films [14]. Linear friction has an important role in the process of the inverse energy cascade since it provides a sink for the energy transferred to large scale, allowing to attain a statistically stationary state [13, 15–18]. The presence of linear damping significantly affects also the statistical properties of the direct enstrophy cascade. Theoretical investigations [19, 20] and numerical simulations [21] of the Ekman-Navier-Stokes equations have shown that the dissipation of enstrophy due to the friction at small scales causes a steepening of the energy spectrum. This results in a correction $\xi > 0$ to the scaling exponent of the spectrum $E(k) \sim k^{-(3+\xi)}$ with respect to the Kraichnan prediction for the direct enstrophy cascade [12]. Theoretical arguments based on the similarities between the process of the direct enstrophy cascade and the chaotic advection of passive scalar fields [19–21] have shown that the correction ξ is determined by the statistics of the stretching rates of the flow and it is proportional to the friction coefficient. More generally, these studies have shown that the friction drag causes the breakdown of self-similar scaling of the vorticity structure functions in the range of scales of the direct enstrophy cascade, resulting in anomalous scaling exponents which depend on the friction coefficient [19, 20]. These relationships provide an intriguing link between the chaoticity of Lagrangian trajectories and the statistical scaling laws in 2D turbulent flows.

In this paper, we pursue the investigation of the effects of linear friction on the direct enstrophy cascade in 2D turbulence by means of a set of high-resolution numerical simulations of the NS equations varying the Reynolds number and friction coefficient. These achievements are made possible by the development of a numerical code specifically designed for single Graphics Processing Unit (GPU) which allows us to greatly speed up the simulation with respect to traditional CPU-based methods. Our findings provide deeper insights into the relationship between the friction and the slope of the energy spectrum showing that the correction ξ displays a universal linear dependence as a function of the friction coefficient rescaled by the characteristic time-scale based on the enstrophy injection rate. We tested the robustness of these results by allowing the development of the inverse energy cascade in the set of simulations with the largest Reynolds number. We also show that fitting the power-law behavior of the enstrophy flux instead of the energy spectrum provides a more accurate measurement of the correction ξ . This method overcomes the difficulties arising from the presence of a logarithmic correction to the spectrum which affects the direct measurement of the correction ξ in the limit of vanishing friction.

The paper is organized as follows: Sec. II provides an overview of the phenomenology of the direct enstrophy cascade in the presence of a linear friction drag, both in the limit of vanishing friction and with finite friction. The results of numerical simulations are discussed in Sec. III. Finally, Sec. IV discusses the implications of our findings and suggests directions for future research. Details on the pseudospectral method and performance benchmarks of our simulations are shown on Appendix A. In Appendix B, we discuss the difficulties on retrieving the scaling exponent from direct measurement of the slope of the energy spectrum, specially in the frictionless limit.

II. DIRECT ENSTROPY CASCADE IN 2D TURBULENCE

The dynamics of an incompressible velocity field $\mathbf{u}(\mathbf{x}, t)$ in two dimensions can be conveniently written in terms of the vorticity field $\omega(\mathbf{x}, t) = \partial_x u_y - \partial_y u_x$ as

$$\partial_t \omega + \mathbf{u} \cdot \nabla \omega = \nu \nabla^2 \omega - \mu \omega + f, \quad (2.1)$$

where ν is the kinematic viscosity and μ is the friction coefficient. The forcing term $f(\mathbf{x}, t) = \partial_x F_y - \partial_y F_x$ is related to the external force field $\mathbf{F}(\mathbf{x}, t)$ which sustain the flow. The forcing field is assumed to be random with a characteristic spatial correlation length of ℓ_f .

In the inviscid, unforced limit, the model (2.1) conserves the kinetic energy $E = \langle |\mathbf{u}|^2 \rangle / 2$ and the enstrophy $Z = \langle \omega^2 \rangle / 2$, where the brackets $\langle (\cdot) \rangle$ indicate the spatial average. In the presence of forcing and dissipation, the energy and enstrophy balances read:

$$\frac{dE}{dt} = -2\nu Z - 2\mu E + \langle \mathbf{u} \cdot \mathbf{F} \rangle = -\varepsilon_\nu - \varepsilon_\mu + \varepsilon_I \quad (2.2)$$

and

$$\frac{dZ}{dt} = -2\nu P - 2\mu Z + \langle \omega f \rangle = -\eta_\nu - \eta_\mu + \eta_I \quad (2.3)$$

where $P = \langle |\nabla \omega|^2 \rangle / 2$ is the so-called palinstrophy that controls viscous dissipation of enstrophy.

The different terms in (2.2-2.3) define, together with the characteristic scales of the forcing $\ell_f = 2\pi\sqrt{\varepsilon_I/\eta_I}$, the viscous dissipation scale $\ell_\nu = 2\pi\sqrt{\varepsilon_\nu/\eta_\nu}$ and the friction scale $\ell_\mu = 2\pi\sqrt{\varepsilon_\mu/\eta_\mu}$. When these scales are well separated, $\ell_\nu \ll \ell_f \ll \ell_\mu$, one expects the development of a direct enstrophy cascade in the inertial range of scales $\ell_\nu \ll \ell \ll \ell_f$ and an inverse energy cascade in the scales $\ell_f \ll \ell \ll \ell_\mu$ [13].

The central statistical object in the classical theory of turbulence is the energy spectrum $E(k)$ defined as $\int E(k)dk = E$ or, equivalently, as $\int k^2 E(k)dk = Z$. The spectral flux of enstrophy $\Pi_Z(k)$ in the direct enstrophy cascade can be related to the energy spectrum according to the following dimensional closure [13]

$$\Pi_Z(k) = \lambda_k E(k) k^3 \quad (2.4)$$

In (2.4), λ_k represents the characteristic frequency of deformation of the eddies at wavenumber k which can be expressed in terms of the energy spectrum as

$$\lambda_k^2 = \int_{k_{min}}^k E(p) p^2 dp \quad (2.5)$$

where $k_{min} = 2\pi/\ell_\mu$ is the minimum wavenumber associated with the largest scale of the flow ℓ_μ . The upper limit in the integral reflects the fact that the fluid motion at scales smaller than $1/k$ acts incoherently, and therefore its average contribution to the deformation rate of the eddies of size $1/k$ vanishes. Considering a scale-invariant energy spectrum $E(k) \propto k^{-\alpha}$, the integral in (2.5) is dominated by the upper limit k provided that the scaling exponent is in the range $\alpha < 3$, satisfying the locality condition [11], and therefore $\lambda_k \simeq E(k)^{1/2} k^{3/2}$.

In the absence of friction ($\mu = 0$), one can assume that the forcing and dissipation terms are both negligible in the enstrophy inertial range, and therefore the flux of enstrophy is constant, $\Pi_Z(k) = \eta$. This assumption, in combination with the dimensional relation (2.4) gives the prediction $E(k) \simeq \eta^{2/3} k^{-3}$. However, this result is not self-consistent because the spectral exponent $\alpha = 3$ is at the border of locality. According to Eq. (2.5), this gives a logarithmic correction for the λ_k and consequently, a non-constant, log-dependent enstrophy flux. A solution to this problem was already proposed by Kraichnan [12]. By taking the derivative of (2.5) and plugging in (2.4) one obtains

$$\Pi_Z(k) = 2k\lambda_k^2 \frac{d\lambda_k}{dk} \quad (2.6)$$

from which, assuming a constant enstrophy flux $\Pi_Z(k) = \eta$, one obtains a log-dependent deformation frequency

$$\lambda_k = \left(\frac{3}{2} \eta \ln \left(\frac{k}{k_f} \right) \right)^{1/3} \quad (2.7)$$

Using this expression in (2.4) one ends with the prediction [12]

$$E(k) \simeq \eta^{2/3} k^{-3} [\ln(k/k_f)]^{-1/3} \quad (2.8)$$

The presence of friction drag changes significantly the whole process of the enstrophy cascade. In particular, it excludes the possibility of a constant flux of enstrophy, causing a steepening of the energy spectrum [19, 20]. This phenomenon can be explained by a simple argument. In the presence of linear friction, from (2.1), one has the following expression for the rate of enstrophy transfer [13]

$$\frac{d\Pi_Z(k)}{dk} = -2\mu k^2 E(k) \quad (2.9)$$

which states that part of the flux is removed in the cascade at a rate proportional to the friction coefficient μ . This causes the steepening of the energy spectrum, with a spectral slope $\alpha > 3$ which exceeds the range of locality. As a consequence, the integral (2.5) is dominated by the contribution of the wavenumbers $k_{min} \leq k \leq k_f$, while the contribution of the wavenumbers $k > k_f$ is negligible, resulting in a constant deformation rate $\lambda_k = \lambda$. Using this assumption in the Eq. (2.4), one immediately obtains the solution

$$E(k) \simeq \frac{\eta}{\lambda} k^{-3} (k/k_f)^{-\xi} \quad (2.10)$$

with the correction to the dimensional scaling exponent

$$\xi = \frac{2\mu}{\lambda}. \quad (2.11)$$

We remark that the above argument can be made more rigorous in the physical space where the role of λ is replaced by the stretching rate of the smooth, chaotic flow. By taking into account the finite-time fluctuations of the stretching rates, one predicts the breakdown of self-similar scaling and the production of intermittency in the statistics of the vorticity field [19] which has been observed in numerical simulations [21].

III. NUMERICAL SIMULATIONS OF THE DIRECT CASCADE WITH FRICTION

We tested the prediction of the previous section, in particular the correction (2.10) to the energy spectrum in the presence of friction by means of extensive direct numerical simulations of Eq. (2.1) at very high resolutions. To accomplish this, we used a pseudo-spectral code implemented on a single GPU. A detailed discussion of the code and its performance can be found in Appendix A.

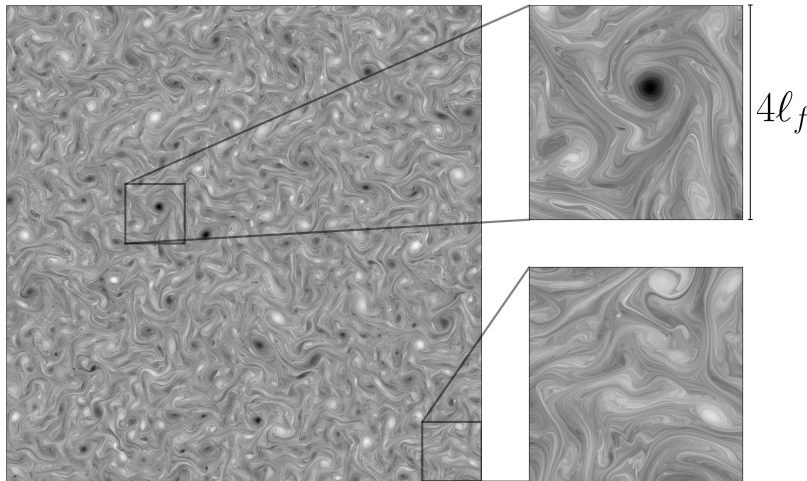


FIG. 1: Snapshot of $\omega(\mathbf{x})$ for Run C with $\mu\eta_I^{-1/3} \approx 0.01$. The upper panel illustrates a region where the flow is dominated by a single, large vortex, approximately the size of the forcing scale. The lower panel depicts a region with no dominant vortices.

Simulations are done in a square box of size $L_x = L_y = 2\pi$, with regular grid of resolution $N = N_x = N_y$. The turbulent flow is sustained by a Gaussian random forcing $f(\mathbf{x}, t)$ with zero mean and white-in-time correlations, acting in a narrow spherical shell of thickness Δk centered at k_f in the wavenumber space. Such a forcing provides an average energy and enstrophy injection rate, ε_I and η_I , respectively, that are related by $\eta_I \approx \varepsilon_I k_f^2$ when $\Delta k \ll k_f$.

Three sets of simulations have been done with different resolutions and viscosities ν , each one covering a large range of friction coefficients μ . By increasing the resolution, we increased the forcing scale to allow the development of a narrow inverse cascade in the simulations at the highest resolution at low friction. Table I reports the most relevant parameters of our simulations. In all cases, small scales are well resolved ($k_{max}\ell_\nu \geq 2.77$). We remark that since the forcing amplitude is kept constant, the enstrophy injection rate increases with the forcing wavenumber and therefore with the resolution.

Fig. 1 shows a snapshot of the vorticity field taken from run C, the highest resolution. The size of the vortices observed in the flow corresponds to the forcing scale, as shown in the upper right panel, which is reduced by increasing the resolution, as indicated in Table I.

The enstrophy balance (2.3) is shown in Fig. 2 for all the simulations in stationary conditions. Remarkably, the curves at different inputs and dissipations collapse when the friction coefficient is made dimensionless with the time-scale associated with the enstrophy injection, i.e. $\tau_I = \eta_I^{-1/3}$. Moreover, we observe from Fig. 2 that for $\mu\eta_I^{-1/3} \gtrsim 0.2$, the

Run	N	ν	$k_f \pm \Delta k$	η_I	Re_ν	$k_{\max} \ell_\nu$	$\mu \times 10^2$
A	4096	2×10^{-5}	8 ± 1	9.615	65584	4.19	1,4,7,10,20,30,40,50,60,80
B	8192	5×10^{-6}	16 ± 1	34.560	100463	3.38	4,6,10,20,30,40,50,60,80,100
C	16384	1.25×10^{-6}	32 ± 1	114.750	149877	2.77	6,12,18,36,48,60,72,96,120

TABLE I: The most relevant parameters of the simulation include $k_f = 2\pi/\ell_f$ and $k_{\max} = N/3$, since we use the 2/3 de-aliasing method. The viscous scale and the Reynolds number are given by $\ell_\nu = \nu^{1/2} \eta_I^{-1/6}$ and $Re = (\ell_\nu/\ell_f)^2$. Both should be taken as lower bound estimates, since if one considers η_ν instead of η_I as the proper dimensional quantity, one obtains strictly larger values for ℓ_ν and Re , since $\eta_\nu < \eta_I$.

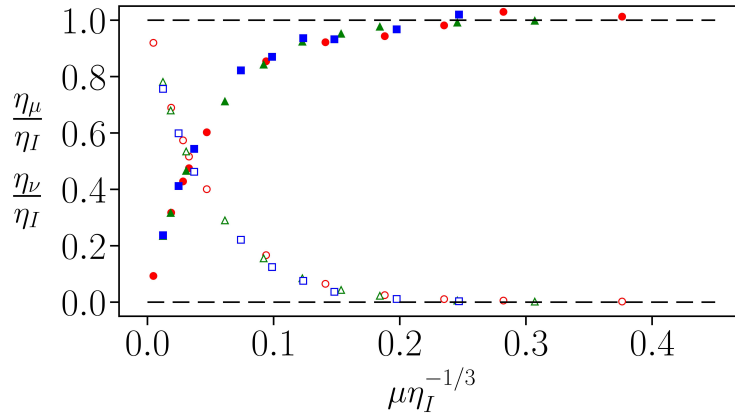


FIG. 2: The ratio of friction dissipation η_μ (filled symbols) and viscous dissipation η_ν (open symbols) to the enstrophy input η_I for the runs A, B, and C are represented by red circles, green triangles, and blue squares, respectively. The friction coefficient is made nondimensional using the timescale associated with η_I .

viscous dissipation is negligible, and the entire enstrophy flux that cascades towards small scales is dissipated by friction before reaching the viscous scale.

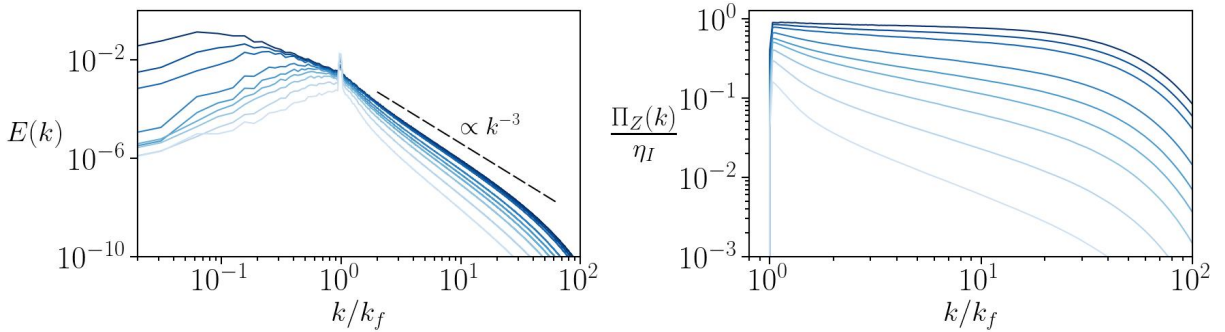


FIG. 3: The left panel shows the energy spectra, while the right panel shows the enstrophy fluxes, both for the simulations of set C. Darker curves correspond to smaller values of μ .

Fig. 3 (left) shows the time-averaged energy spectra for the different simulations of Run

C. In all cases, in the direct cascade range, the spectrum shows a power-law scaling steeper than the simple dimensional prediction $E(k) \propto k^{-3}$ with increasing scaling exponent α for larger friction μ , as expected. The three darker curves, corresponding to smaller friction values, display a short inverse cascade at wavenumber $k < k_f$ with an exponent close to the dimensional prediction for the energy cascade, $k^{-5/3}$. From Fig. 3, it is clear that fitting the scaling exponent α directly from the spectrum is problematic due to the presence of the peak corresponding to the forcing wavenumber. Moreover, in the limit $\mu \rightarrow 0$, the energy spectrum has the logarithmic correction (2.8) to the power-law scaling, and we can expect this to persist for small values of the friction coefficient μ . Indeed, we found empirically that simply fitting the spectra with a power law exponent $3 + \xi$ does not correctly recover the limit $\xi = 0$ for vanishing friction (see Appendix B).

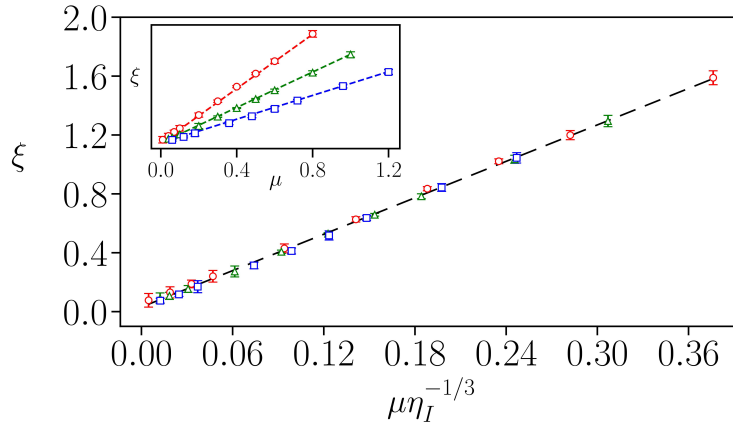


FIG. 4: Spectral correction ξ as a function $\mu\eta_I^{-1/3}$ for simulations A (red circles), B (green triangles), and C (blue squares). The dashed line represents the relation $\xi = a(\mu\eta_I^{-1/3}) + b$ where $a = 4.1 \pm 0.3$ and $b = 0.03 \pm 0.05$. Inset: spectral correction ξ as a function of the dimensional μ for all simulations. Error bars are estimated by varying the fitting range $k_0 \in [3k_f, 5k_f]$ and $k_1 \in [7k_f, 9k_f]$.

To overcome these difficulties, we decided to measure the correction $\xi(\mu)$ directly from the power-law scaling of the flux $\Pi(k)$, since the two quantities are related by (2.9). From the theory, we do not expect logarithmic corrections in the enstrophy flux. The right panel of Fig. 3 shows the spectral enstrophy fluxes for the runs of set C, and we observe a clear power-law scaling in an intermediate range of wavenumbers $k \in [k_0, k_1]$ (with $k_0 \simeq 3k_f$ and $k_1 \simeq 9k_f$), far from the forcing and dissipation scales.

The spectral correction ξ obtained from the power-law fit of the spectral fluxes in the range $k \in [k_0, k_1]$ is shown in Fig. 4. From the inset of Fig. 4, it is evident that the correction $\xi(\mu)$ is proportional to the friction coefficient μ , as predicted by (2.11), with a different slope for the different sets of simulations characterized by varying input. We find that, once again, the correct timescale for non-dimensionalizing the friction parameter is based on the enstrophy input rate. Indeed, as shown in Fig. 4, when plotted as a function of the dimensionless friction coefficient $\mu\eta_I^{-1/3}$, all the data from the different runs collapse onto a single line. Moreover, in the limit $\mu \rightarrow 0$, the spectral correction fitted by the collapsed curve is compatible with zero. We remark that the above rescaling is not the only possibility: one could use $Z^{1/2}$ as an inverse time of the flow, but this would not lead to the data collapsing as shown in Fig. 4.

IV. CONCLUSIONS

In this study, we examined the effects of a linear friction on the direct enstrophy cascade in 2D turbulence using high-resolution numerical simulations of the Navier-Stokes equations. By profiting from a GPU-accelerated code, we explored a wide range of Reynolds numbers and friction coefficients μ uncovering key insights into the dynamics of 2D turbulent flows with linear damping.

Our results confirm that the linear friction introduces a correction ξ to the scaling exponent of the energy spectrum in the direct enstrophy cascade, steepening the dimensionally predicted slope. Theoretically, this correction is expected to scale proportionally to the ratio μ/λ where λ is the average deformation rate of the flow. Our simulations confirmed the scaling $\xi \propto \mu$, providing robust evidence supporting this scaling across a broad parameter space, including different forcing scales, friction coefficients and Reynolds numbers. A precise measure of the correction ξ is obtained from the scaling law of the enstrophy flux and exploiting its relation with the energy spectrum which, in turn, gives less precise results in particular for small values of the friction coefficient. By this procedure, we find that a consistent measure of the deformation rate, in the range of parameters explored here, is expressed in terms of the enstrophy input rate η_I and that $\lambda \propto \eta_I^{1/3}$.

The present result are obtained in a regime of moderate friction, given by the dimensionless coefficient $\mu\eta_I^{-1/3} < 1$. It would be interesting to extend this study to the opposite regime $\mu\eta_I^{-1/3} > 1$, where friction directly affects the statistics of the velocity field at the forcing scale. In such a regime, it is expected that the deformation rate λ depends on μ and therefore we expect a non-linear scaling of the spectral coefficient ξ on the parameters.

Acknowledgement

This work has been supported by Italian Research Center on High Performance Computing Big Data and Quantum Computing (ICSC), project funded by European Union - NextGenerationEU - and National Recovery and Resilience Plan (NRRP) - Mission 4 Component 2 within the activities of Spoke 3 (Astrophysics and Cosmos Observations). We acknowledge HPC CINECA for computing resources within the INFN-CINECA Grant INFN24-fldturb.

Appendix A: Numerical integration of generalized 2D turbulence models

To build numerical solvers for a broader class of turbulent models, we rewrite (2.1) in a more general formulation,

$$(\partial_t + \mathcal{L}_{\nu,\mu}^{n,m})\omega + J(\omega, \psi) = f, \quad (\text{A1})$$

where we introduced a generalized linear dissipative operator,

$$\mathcal{L}_{\nu,\mu}^{n,m} \equiv (-1)^n \nu_{2n} \nabla^{2(n+1)} + (-1)^m \mu_{2m} \nabla^{-2m}, \quad (\text{A2})$$

representing a positive-diagonal operator in the Fourier space $\hat{\mathcal{L}}_{\nu,\mu}^{n,m}(k) = \nu_{2n} k^{2(n+1)} + \mu_{2m} k^{-2m}$. Although this paper is devoted to the study of the direct cascade in 2D NS turbulence, the equation (A1) contains a whole class of turbulence models known as α -turbulence [22]. The definition of this class of model is better understood through the relation between

the generalized vorticity $\omega(\mathbf{x}, t)$ and the stream function $\psi(\mathbf{x}, t)$, represented in the Fourier space through

$$\hat{\omega}(\mathbf{k}, t) = |\mathbf{k}|^\alpha \hat{\psi}(\mathbf{k}, t) . \quad (\text{A3})$$

In the following, we will discuss the case $\alpha = 2$ but the scheme can be adapted to any value of α .

The generalized dissipative operator has the role discussed in Section II, i.e. to provide stationary states and prevent condensate formations. For $m = n = 0$ one recovers the standard friction/viscosity terms. In comparison, for $m, n > 0$ depending on the orders n and m of the dissipative operator, the coefficients μ and ν have different dimensional roles and can dissipate over a more narrow range of scales. For example, hyperviscosity ($n > 0$) is used to diminish the action of dissipation on the dissipative subrange, leading to extended inertial ranges at the cost of a bigger thermalization effect (bottleneck) of high wavenumber [23, 24]. Moreover, one reason to introduce hypofriction ($m > 0$) instead of normal friction is to avoid the correction to the enstrophy cascade discussed in Section II.

We developed and tested an original pseudospectral code to integrate the general model on Nvidia hardware. Pseudospectral schemes are widely used in numerical studies of turbulence because of their accuracy in derivatives and the simplicity of inverting the Laplace equation. Another practical advantage is that most of the resources in the pseudospectral scheme are used to compute the Fast Fourier Transforms (FFT) necessary to move back and forth from Fourier space (where derivatives are computed) to physical space (where products and other nonlinear terms are evaluated). Therefore, to make the code efficient for a given architecture, it is (almost) sufficient to have an efficient FFT.

The numerical code gTurbo2D uses a standard Runge-Kutta (RK) scheme to time advance the solution with exact integration of the linear terms. In the simple case of a second-order RK scheme, the evolution of the vorticity field in (A1) is given by

$$\hat{\omega}(\mathbf{k}, t + dt) = e^{-\hat{\mathcal{L}}dt} \hat{\omega}(\mathbf{k}, t) + e^{-\hat{\mathcal{L}}dt/2} \hat{N} \left(e^{-\hat{\mathcal{L}}dt/2} \hat{\omega}' \right) dt \quad (\text{A4})$$

where $\hat{(\cdot)}$ represents the Fourier transformed fields and

$$\hat{\omega}' = \hat{\omega}(\mathbf{k}, t) + \hat{N}(\hat{\omega}(\mathbf{k}, t)) dt/2 \quad (\text{A5})$$

The evaluation of the nonlinear term \hat{N} is partially done in the physical space (to avoid the computation of convolutions). In the present implementation of the code, the evaluation of the nonlinear term is done as follows. From the vorticity field in Fourier space, the code computes the stream function by inverting (A3). The two components of the velocity \hat{v}_i are then obtained from the derivatives of $\hat{\psi}$ and then transformed in the physical space together with the vorticity (this step requires 3 inverse FFTs). The products $(v_i \omega)$ are computed (and stored in the same arrays of the velocity) and transformed back in Fourier space (this requires 2 direct FFTs). Finally, the divergence of $(v_i \hat{\omega})$ is computed and stored in the original array. Therefore the evaluation of the nonlinear term requires 5 FFTs and each step of the n -order RK scheme requires $5n$ FFTs.

The code gTurbo2D is written in Fortran 90 with OpenACC, which enables the use of Nvidia hardware through compiler directives. For the FFTs, the code makes massive use of the cuda FFT library, compatible with the OpenACC programming paradigm. Simulations are performed on *Leonardo* machine, a pre-exascale Tier-0 supercomputer where, each of the 3456 computing nodes is composed of a single-socket processor of 32-core at 2.60GHz, 512

GB of RAM and, 4 Nvidia A100 GPUs of 64GB each connected by NVLink 3.0. The version of gTurbo2D used for this work is a single GPU code while the multi-GPU version is under development. We remark that the study of 2D turbulence requires much less memory than 3D (a single scalar field in two dimensions) and the remarkable resolution of $N^2 = 32768^2$ grid points can be reached on a single GPU. However, large resolutions require very small time steps and therefore the resolution is limited not only by the memory but also by the speed of the code.

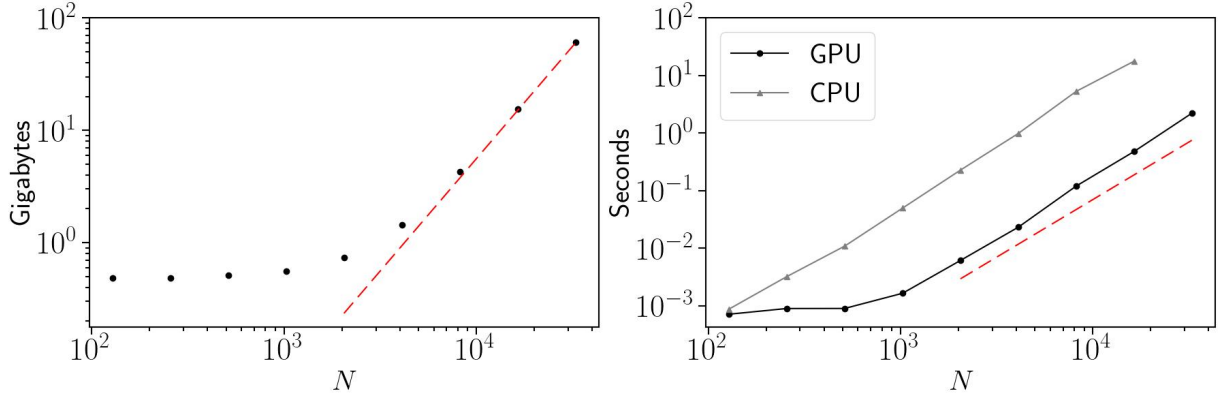


FIG. 5: Left panel shows GPU's memory usage while right panel shows mean elapsed time (computed with 1000 timesteps) as functions of the resolution. Red dashed line shows N^2 scaling.

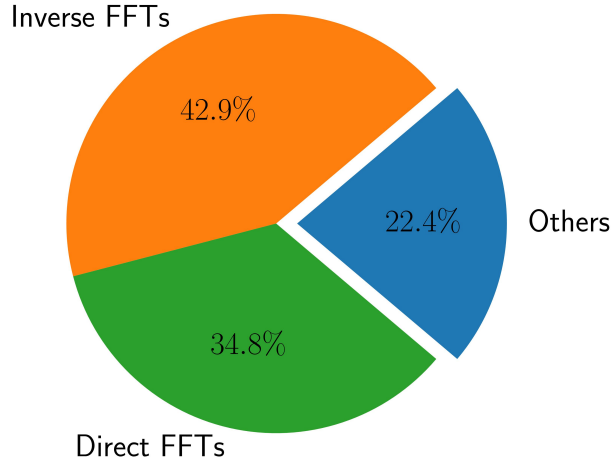


FIG. 6: Representative graph of the time fraction allocated to each stage in the code.

The left panel of Fig. 5 shows the total GPU memory usage in Gb (circles) as a function of the resolution N . For moderate resolution $N \lesssim 2000$ the memory usage is almost independent of the resolution since most of the memory is used to store the libraries, the kernel, and the resolution-independent variables. For larger resolutions, the memory used to store the 2D fields dominates and therefore it is proportional to N^2 . Remarkably, we observe a similar behavior for the mean elapsed time. This can be explained by the relative smallness

of the problem compared to the GPU parallelization capacity. Indeed, not all the registers on the GPUs are required to fully parallelize the computation which therefore is performed in a time independent of the resolution. For larger resolution, the computational time grows proportionally to the amount of computation required for the time step, i.e. to N^2 .

Fig. 6 shows the percentage of time spent on the simulation for each RK cycle at the maximum resolution ($N^2 = 32768^2$). One should note that the most computationally intensive part is due to the forward and backward FFTs (steps 2 and 4) that account for more than 75% of the computational time. However, the importance of the forward and backward transforms is different since their subroutines are called with different frequencies. Besides, we decided to move the normalization to the forward transform since it has fewer calls per timestep. Although the integrator stability depends intrinsically on the physical properties of the system in question, we observed some practical advantages of using RK4 in some tested cases for simulations with fixed physical time $T = N_t dt$, since higher order schemes can allow one to use larger timesteps.

Appendix B: The effect of the log correction when measuring spectral correction

To measure the correction $\xi(\mu)$, we first analyze the spectrum $E(k)$ under the assumption of a pure power-law scaling, $E(k) \propto k^{-3-\xi}$. The result is shown in Fig. 7 where we observe a vertical shift in the y-axis which is incompatible with the arguments put forward in Sec. II. In particular, the limit $\xi(\mu \rightarrow 0) \rightarrow 0$ is completely missed even when the error bars are huge, which is the case of low-resolution simulations.

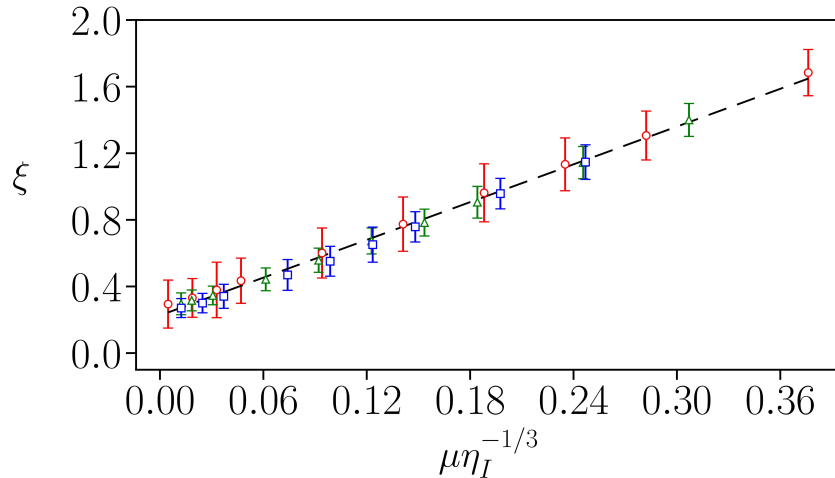


FIG. 7: Same as Fig. 4 with ξ fitted directly from the spectra. The dashed line represents the relation $\xi = a(\mu\eta_I^{-1/3}) + b$ where $a = 3.8 \pm 0.5$ and $b = 0.22 \pm 0.08$.

We tested the validity of Eq. (2.4) for the case where $\lambda_k = \lambda_{k_f}$. This equation predicts $E(k)k^3/\Pi_Z(k) \approx \text{const.}$ in the enstrophy inertial range. Fig. 8 shows this relation as functions of the wavenumber k for a simulation with a small value of $\mu\eta_I^{-1/3}$. The darker curve includes the log correction term $\ln(k/k_f)^{1/3}$ as in Eq. (2.9) while the lighter curve shows simply Eq. (2.4). By Fig. 8, one should note that for small friction, there exists an emergent logarithmic correction to the deformation frequency which is the source of our difficulties in

fitting the correct scaling exponent through the spectrum. Indeed, if one fits the spectrum taking into account the correction the offset vanishes (not shown). However, this procedure

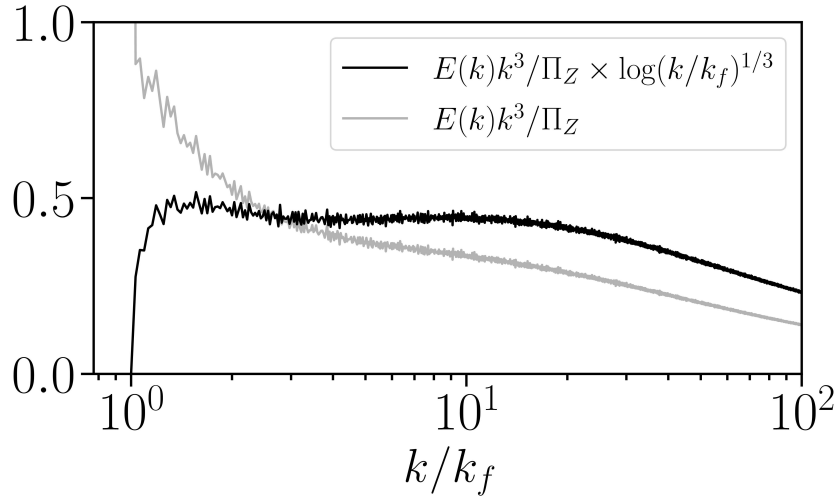


FIG. 8: Test for the dimensional relation (2.4) for a simulation on Run C with $\mu\eta_I^{-1/3} \approx 0.04$.

cannot be systematically applied for all values of μ since we expect the logarithmic correction to be less pronounced for large friction. Then, we decided to extract the correction directly from the flux $\Pi_Z(k)$ since it is not supposed to present the logarithmic term. This procedure also showed to reduce error bars for all simulations (see Figs. 4 and 7).

-
- [1] G. K. Vallis, *Atmospheric and oceanic fluid dynamics* (Cambridge University Press, Cambridge, 2017).
 - [2] G. Lapeyre and P. Klein, *J. Phys. Oceanogr.* **36**, 165 (2006).
 - [3] L. Siegelman, P. Klein, A. P. Ingersoll, S. P. Ewald, W. R. Young, A. Bracco, A. Mura, A. Adriani, D. Grassi, C. Plainaki, et al., *Nat. Phys.* **18**, 357 (2022).
 - [4] M. Jukes, *J. Atmos. Sci.* **51**, 2756 (1994).
 - [5] H. Xia, M. Shats, and G. Falkovich, *Phys. Fluids* **21** (2009).
 - [6] S. J. Benavides and A. Alexakis, *J. Fluid Mech.* **822**, 364 (2017).
 - [7] S. Musacchio and G. Boffetta, *Phys. Rev. Fluids* **4**, 022602 (2019).
 - [8] H.-Y. Zhu, J.-H. Xie, K.-Q. Xia, et al., *Phys. Rev. Lett.* **130**, 214001 (2023).
 - [9] H. K. Moffatt, *Magnetic field generation in electrically conducting fluids* (Cambridge University Press, Cambridge, 1978).
 - [10] A. N. Kolmogorov, *Dokl. Akad. Nauk SSSR* **30**, 301 (1941).
 - [11] U. Frisch, *Turbulence: the legacy of A.N. Kolmogorov* (Cambridge University Press, Cambridge, 1995).
 - [12] R. H. Kraichnan, *J. Fluid Mech.* **47**, 525 (1971).
 - [13] G. Boffetta and R. E. Ecke, *Annu. Rev. Fluid Mech.* **44**, 427 (2012).
 - [14] M. Rivera and X.-L. Wu, *Phys. Rev. Lett.* **85**, 976 (2000).
 - [15] R. H. Kraichnan, *Phys. Fluids* **10**, 1417 (1967).
 - [16] C. E. Leith, *Phys. Fluids* **11**, 671 (1968).

- [17] G. K. Batchelor, *Phys. Fluids* **12**, II (1969).
- [18] M. Chertkov, C. Connaughton, I. Kolokolov, and V. Lebedev, *Phys. Rev. Lett.* **99**, 084501 (2007).
- [19] K. Nam, E. Ott, T. M. Antonsen Jr, and P. N. Guzdar, *Phys. Rev. Lett.* **84**, 5134 (2000).
- [20] D. Bernard, *Europhys. Lett.* **50**, 333 (2000).
- [21] G. Boffetta, A. Celani, S. Musacchio, and M. Vergassola, *Phys. Rev. E* **66**, 026304 (2002).
- [22] R. T. Pierrehumbert, I. M. Held, and K. L. Swanson, *Chaos Solit. Fract.* **4**, 1111 (1994).
- [23] N. E. L. Haugen and A. Brandenburg, *Phys. Rev. E* **70**, 026405 (2004).
- [24] U. Frisch, S. Kurien, R. Pandit, W. Pauls, S. S. Ray, A. Wirth, and J.-Z. Zhu, *Phys. Rev. Lett.* **101**, 144501 (2008).